

Dynamical instabilities for model with point-coupling interactions: Vlasov formalism method

Yanjun Chen^{1,2,*}, Juan Zou¹, Zipeng Cheng¹, and Binguang He¹

¹ *Department of Physics and Electronic Science,*

Changsha University of Science and Technology, Changsha, Hunan 410114, China

² *Hunan Provincial Key Laboratory of Flexible Electronic*

Materials Genome Engineering, Changsha, Hunan 410114, China

Abstract

We explore the effects of the density dependence of symmetry energy on the dynamical instabilities and crust-core phase transition in the cold and warm neutron stars in the RMF theory with point-coupling interactions using the Vlasov approach. The role of the temperature and neutrino trapping has also been considered. The distillation effect, crust-core transition density and pressure, the cluster size and growth rates have been discussed. The present work shows that the slope of symmetry energy, temperature, and neutrino trapping have obvious effects.

PACS numbers: 21.60.Ev, 21.30.Fe, 26.60.-c, 26.60.Gj, 21.65.Cd

*Electronic address: chenyjy@ustc.edu.cn

I. INTRODUCTION

Neutron stars (NS) consist of a solid crust at low densities and a homogeneous core in liquid phase. It is known that the uniform liquid becomes unstable against small-amplitude density oscillations when the density decreases from the high-density homogeneous core to the inhomogeneous crust. Consequently, the phase transitions occur which are associated to the liquid-gas phase transition in asymmetric nuclear matter in the presence of electrons. It is indicated that the properties of the crust and core-crust phase transition play the important role in understanding some astrophysical observations [1–5].

It is well known that the relativistic mean field (RMF) theory can successfully describe many nuclear phenomena and explain the saturation mechanism of nuclear matter and the strong spin-orbit interaction in finite nuclei in a consistent way [6–10]. In recent years, instead of the traditional RMF theory that is based on the effective interaction between Dirac nucleons via the exchange of mesons, the RMF model with point-coupling (PC) interactions [11–13], which neglects mesonic degrees of freedom and considers only interactions with zero range, has become an alternative approach for the description of nuclear matter and finite nuclei. It allows a simpler treatment of exchange terms to study the effects beyond the mean-field for nuclear low-lying collective excited states, and provides more opportunities to investigate the relationship to the non-relativistic approaches.

Ref. [14] has used a widely used density-dependent parametrization of PC model, DD-PC1 [12], to study the core-crust transition density at zero temperature within the thermodynamical approach and the effects of the density dependence of symmetry energy. In this work, based on the parametrization DD-PC1, we use the Vlasov formalism method, which is widely used to study the stability of NS matter and the core-crust transition within various models [15–22], to investigate the effects of the density dependence of the symmetry energy on the dynamical instabilities and phase transitions expected in the neutron star crust, considering the influences of finite temperature and neutrino trapping as well. The spectrum of collective modes, or the dispersion relation of the system in the Vlasov approach arises from small oscillations around the equilibrium state. The unstable collective modes are characterized by an imaginary frequency of the dispersion relation. Thus, the Vlasov formalism method, which incorporates the surface and Coulomb effects, is more realistic than the thermodynamical one which corresponds to the situation with the wave vector of

collective modes tending to zero.

This article is organized as follows. In Sec. II, we describe the formulas necessary for the present work. In Sec. III, the calculated results and some discussions are given. Finally, the summary is present in Sec. IV.

II. THE FORMALISM

In this work, the Lagrangian for DD-PC1 parametrization reads

$$L = \bar{\psi}[\gamma^\mu(i\partial_\mu - eA_\mu\frac{1-\tau_3}{2}) - M]\psi - \frac{1}{2}\alpha_S(\hat{\rho})(\bar{\psi}\psi)(\bar{\psi}\psi) - \frac{1}{2}\delta_S(\partial_\nu\bar{\psi}\psi)(\partial^\nu\bar{\psi}\psi) - \frac{1}{2}\alpha_V(\hat{\rho})(\bar{\psi}\gamma^\mu\psi)(\bar{\psi}\gamma_\mu\psi) - \frac{1}{2}\alpha_{tV}(\hat{\rho})(\bar{\psi}\vec{\tau}\gamma^\mu\psi) \cdot (\bar{\psi}\vec{\tau}\gamma_\mu\psi) , \quad (1)$$

where ψ is the Dirac spinor of baryons and A_μ denotes the electromagnetic field. The coupling parameter δ is considered to be constant, while α 's in the various spin-isospin channels are analytical functions with respect to the baryonic density ρ alone, given by $\alpha_i = a_i + (b_i + c_i x)e^{-d_i x}$ in which $x = \rho/\rho_{sat}$, and ρ_{sat} denotes the saturation density of symmetric nuclear matter. The original DD-PC1 parameter sets are listed in Table I.

The effective one-body Hamiltonian can be given by

$$h_i = \begin{cases} \sqrt{M^{*2} + (\vec{p} - \vec{V}_i)^2} + V_i^0 , & \text{for } i = p, n , \\ \sqrt{m_e^2 + (\vec{p} + e\vec{A})^2} - eA_0 , & \text{for } i = e , \end{cases} \quad (2)$$

where the nucleon effective mass is defined as $M^* = M + \Sigma_S$, and the scalar and vector self-energies, Σ_S and $V^\mu = \Sigma_V^\mu + \Sigma_R^\mu$, in which the rearrangement term Σ_R^μ arises from the variation of the density-dependent vertex functionals with respect to the nucleon fields in the density operators, can be given by

$$\Sigma_S = \alpha_S \rho_S - \delta_S \Delta \rho_S , \quad (3)$$

$$\Sigma_V^\mu = \alpha_V j^\mu + \alpha_{tV} \tau_i j_3^\mu + e \frac{1 + \tau_i}{2} A^\mu , \quad (4)$$

$$\Sigma_R^\mu = (\alpha'_S \rho_S^2 + \alpha'_V j_\nu j^\nu + \alpha'_{tV} j_{3\nu} j_3^\nu) j^\mu / 2\rho_V , \quad (5)$$

The Vlasov equation describes the time evolution of the one-body phase-space distribution functions for protons, neutrons, and electrons, denoted by $f_{i\pm}(\vec{r}, \vec{p}, t)$, as

$$\frac{\partial f_{i\pm}}{\partial t} + \{f_{i\pm}, h_{i\pm}\} = 0 , \quad i = p, n, e, \quad (6)$$

where $+(-)$ denotes particles (antiparticles), and $\{ , \}$ denotes the Poisson brackets. Small deviations of the distribution functions δf around the equilibrium state can be obtained with generating functions S as

$$\delta f_{i\pm} = \{S_{i\pm}, f_{0i\pm}\} = \{S_{i\pm}, p^2\} \frac{df_{0i\pm}}{dp^2}, \quad (7)$$

where f_{0i} are equilibrium distribution functions. Of particular interest are the longitudinal modes, with momentum \vec{k} and frequency ω , described by the ansatz

$$\begin{pmatrix} S_{i\pm}(\vec{r}, \vec{p}, t) \\ \delta\Sigma_S, \delta V^\mu \\ \delta\rho_S, \delta j^\mu, \delta j_3^\mu \\ \delta A^\mu \end{pmatrix} = \begin{pmatrix} S_{\omega\pm}^i(p, \cos\theta) \\ \delta\Sigma_\omega^S, \delta V_\omega^\mu \\ \delta\rho_\omega^S, \delta j_\omega^\mu, \delta j_{3\omega}^\mu \\ \delta A_\omega^\mu \end{pmatrix} e^{i(\omega t - \vec{k} \cdot \vec{r})}, \quad (8)$$

where θ is the angle between \vec{p} and \vec{k} . In terms of the generating functions, the linearized Vlasov equations for δf can be obtained. After transforming the unknowns S_ω to the density oscillations, we obtain

$$\begin{aligned} \delta\rho_{\omega i} &= \frac{2}{(2\pi)^3} \int d^3p (\delta f_{i+} - \delta f_{i-}) \\ &= \frac{-1}{2\pi^2 T} [M^* \delta\Sigma_\omega^{Si} (I_{\omega+}^{1i} + I_{\omega-}^{1i}) + \delta V_\omega^{0i} (I_{\omega+}^{2i} - I_{\omega-}^{2i}) - \frac{\omega}{k} \delta V_\omega^i (I_{\omega+}^{2i} - I_{\omega-}^{2i})], \quad i = p, n \end{aligned} \quad (9)$$

$$\begin{aligned} \delta\rho_{\omega S} &= \frac{2}{(2\pi)^3} \left[\int d^3p (\delta f_{i+} + \delta f_{i-}) \frac{M^*}{\epsilon} + \int d^3p (f_{0i+} + f_{0i-}) \delta\left(\frac{M^*}{\epsilon}\right) \right] \\ &= \frac{-M^*}{2\pi^2 T} [M^* \delta\Sigma_\omega^{Si} (I_{\omega+}^{0i} - I_{\omega-}^{0i}) + \delta V_\omega^{0i} (I_{\omega+}^{1i} + I_{\omega-}^{1i}) - \frac{\omega}{k} \delta V_\omega^i (I_{\omega+}^{1i} + I_{\omega-}^{1i})] \\ &\quad + \frac{2}{(2\pi)^3} \int d^3p (f_{0i+} + f_{0i-}) \delta\left(\frac{M^*}{\epsilon}\right), \quad i = p, n \end{aligned} \quad (10)$$

and

$$\delta\rho_{\omega e} = \frac{e\delta A_\omega^0}{2\pi^2 T} (I_{\omega+}^{2e} - I_{\omega-}^{2e}) (1 - \omega^2/k^2), \quad (11)$$

in which

$$(\omega^2 - k^2) \delta A_\omega^0 = -e(\delta\rho_{\omega p} - \delta\rho_{\omega e}), \quad (12)$$

and

$$I_{\omega\mp}^{ni} = \int_{m_i}^{\infty} \epsilon^n I_{\omega\mp}(\epsilon) f_{0i\mp} (f_{0i\mp} - 1) d\epsilon, \quad (13)$$

with

$$I_{\omega\mp}(\epsilon) = \int_{-p/\epsilon}^{p/\epsilon} dx \frac{x}{\omega/k \pm x} . \quad (14)$$

Here m_i means M^* for nucleon and m_e for electron, $\delta\rho_{\omega p}^S$ and $\delta\rho_{\omega n}^S$ are the amplitudes of the oscillating scalar densities of protons and neutrons, respectively, and $\delta\rho_{\omega p}$, $\delta\rho_{\omega n}$, and $\delta\rho_{\omega e}$ are the amplitudes of the oscillating proton, neutron, and electron densities. For zero temperature, Eqs. 9-14 can still be applied in the present work when one replaces $I_{\omega\mp}^{ni}$ given by

$$I_{\omega-}^{ni} = 0 , \frac{I_{\omega+}^{ni}}{T} \Rightarrow -\epsilon_{iF}^n I_{\omega+}(\epsilon_{iF}) , \quad (15)$$

in which T is the temperature and ϵ_F is the Fermi energy at zero temperature. After some derivation, including the equation of motion of photons where the protons and electrons are sources of Coulomb potential, Eqs. 9-11 can easily be put into a matrix form as

$$M(\omega) \begin{pmatrix} \delta\rho_{\omega p}^S \\ \delta\rho_{\omega n}^S \\ \delta\rho_{\omega p} \\ \delta\rho_{\omega n} \\ \delta\rho_{\omega e} \end{pmatrix} = 0 , \quad (16)$$

Then the dispersion relation of collective modes is obtained from the determinant of $M(\omega)$. Eqs. 9-15 are the universal equations for the investigation within the Vlasov approach. It is worth pointing out that for the zero-range PC RMF models, Eqs. 9-10 are the functions with respect of the oscillating scalar and baryon densities, thus can directly be put into the matrix form as Eq. 16, while for the finite-range meson-exchange RMF models, Eqs. 9-10 are the functions with respect of the oscillating meson fields, and one has to use the equations of motion of mesons to replace the oscillating meson fields in Eqs. 9-10 by the oscillating densities.

III. RESULTS AND DISCUSSION

In this work, the parameters of isoscalar channels in the Lagrangian Eq. 1 remain unchanged in order that the properties of the saturated symmetric nuclear matter, namely, the

saturation density, the binding energy, and the compression modulus, are kept fixed. We vary the density dependence of symmetry energy by adjusting the parameters of isovector channels, i.e., b_{tV} and d_{tV} , in Eq. 1 and Table I, while keeping the symmetry energy at saturation unchanged which is 33 MeV for DD-PC1.

It is known that the unstable modes correspond to the solutions of the dispersion relation with imaginary frequencies $\omega = i\Gamma$, where Γ defines the exponential growth rate of the instabilities. With these solutions, we study the instability direction of the modes and the distillation effect, i.e., the denser phase in nonhomogeneous nuclear matter prefers to be isospin symmetric. We plot the ratio of the proton over neutron density fluctuation $\delta\rho_p/\delta\rho_n$ as a function of the wave vector \vec{k} and the density ρ in Fig. 1 and Fig. 2, respectively, for the proton fraction $y_p = 0.3$ which is close to that in β -equilibrium matter with neutrino trapping at $T = 4$ MeV. Fig. 1 shows that for the largest density considered, i.e., $\rho = 0.5\rho_0$, the different slopes of symmetry energy at saturation (parameter L) give rise to obviously distinct results, specifically, large L corresponding to large distillation effect. With decreasing densities, the opposite behavior is found. The phenomenon can be seen in Fig. 2 more obviously. Fig. 2 shows that for $\rho \gtrsim 0.05 \text{ fm}^{-3}$, the large L increases the distillation effect, while at lower densities, the opposite occurs, i.e., lower L results in larger $\delta\rho_p/\delta\rho_n$. It indicates that in the nonhomogeneous region near the inner boundary of the crust, where the densities are above a value, e.g., about 0.05 fm^{-3} in this case, the clusters prefer more proton rich for larger L , while in the lower-density region of the crust, the larger L prefers the clusters with more neutron rich.

In Tables II-III, we show the transition densities n_t and corresponding pressures P_t at the crust-core transition in β -equilibrium neutron star matter for several values of L , respectively. The values in both tables are for several temperatures with free ($Y_\nu = 0$) and trapped ($Y_l = 0.4$) neutrinos. The transition is defined as the crossing between the β -equilibrium line and the spinodal surface. The thermodynamical spinodal region requires the free energy curvature matrix is negative, while the Vlasov spinodal surface corresponds to the solutions of the dispersion relation with the frequency $\omega = 0$ and the moment $k = 75 \text{ MeV}$ where the chosen value of k in this work approximately defines the maximal spinodal region. For the original DD-PC1 parametrization, the calculated n_t for $T = 0 \text{ MeV}$ with thermodynamical method are 0.079 and 0.093 fm^{-3} for neutrino-free and neutrino-trapped β -equilibrium matter, respectively, while they are about 10% smaller for Vlasov formalism method, which

accordingly are 0.072 and 0.084 fm^{-3} , respectively. The anticorrelation of n_t and the slope L has been found in the literature using various methods [23–31]. Similarly, one sees in Table II that small L corresponds to the great value of n_t . It can also be seen that n_t decreases with temperature. Moreover, in the crust of neutrino-free matter, we see that there is no nonhomogeneous phase at temperatures above 4 MeV for $L > 70$ MeV, and even for very low L , no nonhomogeneous phase exists at $T = 12$ MeV. This mainly results from the fact that the spinodal region can almost reach pure neutron matter at zero temperature while it is more isospin symmetric for finite temperature (see Fig. 1 of Ref. [16]). Meanwhile, the proton fraction of β -equilibrium neutrino-free matter is quite small at subsaturation and the β -equilibrium line can only pass across the spinodal region marginally. Thus the crust-core transition is susceptible to the changes of temperature. It is known that the greater L corresponds to smaller symmetry energy at subsaturation densities and favors more neutron-rich matter for homogeneous phase at subsaturation. As a result, the nonhomogeneous phase can only exist at low temperature for great L . As a contrast, the proton fraction in the matter with trapped neutrinos is quite large, ~ 0.3 . Therefore, Table II shows that the transition densities do not differ much for various L and the nonhomogeneous phase still exists until $T = 12$ MeV. It means that the nonhomogeneous phase can exist at higher temperature in the crust of the proton-neutron star compared with that after neutrinos outflow. In contrast with n_t , the dependence of P_t on the slope L is nontrivial, as shown in Table III. At $T = 0$ MeV, for $Y_\nu = 0$, P_t increases with increasing L for small L region ($L \lesssim 55$ MeV) and the opposite behavior occurs for $L \gtrsim 55$ MeV. This trend is similar to that observed in Ref. [21, 28, 29], while not to that in Ref. [27, 31]. For $Y_l = 0.4$, the trend for thermodynamical method is different and P_t increases monotonically with increasing L . Moreover, it is observed that P_t can become downward with increasing L when temperature increases. These phenomena might come from several competing effects, as discussed in Ref. [28, 29], and can be model dependence.

The most unstable mode is taken as the mode with the largest growth rate $|\omega|_{max}$, which drives the matter to the nonhomogeneous phase. Half of the wavelength $\lambda_{max}/2$ associated with this mode is related to the most probable size of the clusters that are formed by the perturbation. We plot $|\omega|_{max}$ (upper panels) and corresponding $\lambda_{max}/2$ (lower panels) as a function of density for $T = 0$ MeV and several different finite temperatures, $T = 4, 8,$ and 12 MeV in β -equilibrium matter without neutrinos in Fig. 3 and considering neutrino

trapping with a lepton fraction $Y_l = 0.4$ in Fig. 4. We see from Fig. 3 that except for very low densities, e.g., $\rho \lesssim 0.02 \text{ fm}^{-3}$, the smaller the slope L , the larger the growth rate and the smaller the size of the clusters. It is seen that both the largest value of the growth rates and the smallest size of the clusters are shifted to larger densities when L decreases. Moreover, the density range for instabilities increases with decreasing L . These phenomenons can also be seen in Fig. 4. However, we see the differences between various L in Fig. 4 are small. It can be explained by the large proton fraction for matter with trapped neutrinos. The figures show that the effects of the temperature are large and globally to reduce the instability region and the growth rate and to increase the cluster size. The largest growth rate and the smallest clusters are also observed to shift to larger densities with increasing temperature. For neutrino-free matter, there is no cluster in Fig. 3 at temperatures above 4 MeV for $L \gtrsim 70 \text{ MeV}$, while the clusters still exist at $T = 12 \text{ MeV}$ in Fig. 4 for matter with trapped neutrinos. Comparing these two figures, we see that the neutrino trapping leads to larger growth rate and smaller clusters, e.g., The smallest size of clusters is about 4 MeV for neutrino-free matter, while $\sim 3 \text{ MeV}$ when including neutrinos.

IV. SUMMARY

In summary, based on the universal equations Eqs. 9-15, we have used the Vlasov formalism method to explore the effects of the density dependence of symmetry energy on the dynamical instabilities and crust-core phase transition in the cold and warm neutron stars in the RMF theory with PC interactions. The role of the temperature and neutrino trapping has also been considered. We see that the clusters in the nonhomogeneous region near the inner boundary of the crust prefer more proton rich for larger L at $\rho \gtrsim 0.05 \text{ fm}^{-3}$, while in the lower-density region of the crust, the larger L prefers the clusters with more neutron rich. It is seen that n_t decreases when the slope L or the temperature increases. For β -equilibrium neutrino-free matter, the crust-core transition is susceptible to the changes of temperature. The nonhomogeneous phase can only exist at low temperature for great L . Even for very low L , no nonhomogeneous phase exists at $T = 12 \text{ MeV}$. As a contrast, the nonhomogeneous phase still exists until $T = 12 \text{ MeV}$ in the matter with trapped neutrinos and the transition densities do not differ much for various L due to the large proton fraction. In contrast with n_t , the dependence of the transition pressure P_t on the slope L is nontrivial. At $T = 0$

MeV, for $Y_\nu = 0$, P_t increases with increasing L for $L \lesssim 55$ MeV and the opposite behavior occurs for $L \gtrsim 55$ MeV, whereas for $Y_l = 0.4$, the trend for thermodynamical method is different which increases monotonically with increasing L . When temperature increases, P_t can become downward with increasing L .

The slope of symmetry energy, temperature, and trapping neutrinos have obvious effects on the estimated size of clusters and growth rates. The small L corresponds to small cluster size, large growth rate and large density range for instabilities. The temperature reduces the instability region and growth rate and increases the cluster size. Moreover, the largest growth rate and the smallest clusters are shifted to larger densities with decreasing L or increasing temperature. The neutrino trapping can reduce the effects of L due to the large proton fraction and leads to large growth rate and small clusters.

Acknowledgments

The authors would like to thank the anonymous referee for her/his constructive suggestions which are very helpful to improve this manuscript.

-
- [1] B. Link, R.I. Epstein, and J.M. Lattimer, *Phys. Rev. Lett.* **83**, 3362 (1999)
- [2] N. Andersson, K. Glampedakis, W. Ho, and C. Espinoza, *Phys. Rev. Lett.* **109**, 241103 (2012)
- [3] N. Chamel, *Phys. Rev. Lett.* **110**, 011101 (2013)
- [4] J.M. Lattimer and Y. Lim, *Astrophys. J* **771**, 51 (2013)
- [5] J. Piekarewicz, F.J. Fattoyev, and C.J. Horowitz, *Phys. Rev. C* **90**, 015803 (2014)
- [6] B.D. Serot, and J.D. Walecka, in *Advances in Nuclear Physics*, edited by J.W. Negele, and E. Vogt, (Plenum Press, New York, 1986), **16**, 1
- [7] P.G. Reinhard, *Rep. Prog. Phys.* **1**, 147 (1989)
- [8] P. Ring, *Prog. Part. Nucl. Phys.* **37**, 193 (1996)
- [9] M. Bender, P.H. Heenen, and P.G. Reinhard, *Rev. Mod. Phys.* **75**, 121 (2003)
- [10] J. Meng, H. Toki, S.G. Zhou, S.Q. Zhang, W.H. Long, and L.S. Geng, *Prog. Part. Nucl. Phys.* **57**, 470 (2006)
- [11] T. Bürvenich, D.G. Madland, J.A. Maruhn, and P.-G. Reinhard, *Phys. Rev. C* **65**, 044308 (2002)
- [12] T. Nikšić, D. Vretenar, and P. Ring, *Phys. Rev. C* **78**, 034318 (2008)
- [13] P.W. Zhao, Z.P. Li, J.M. Yao, and J. Meng, *Phys. Rev. C* **82**, 054319 (2010)
- [14] Ch.C. Moustakidis, T. Nikšić, G.A. Lalazissis, D. Vretenar, and P. Ring, *Phys. Rev. C* **81**, 065803 (2010)
- [15] C. Providência, L. Brito, S.S. Avancini, D.P. Menezes, and Ph. Chomaz, *Phys. Rev. C* **73**, 025805 (2006)
- [16] L. Brito, C. Providência, A.M. Santos, S.S. Avancini, D.P. Menezes, and Ph. Chomaz, *Phys. Rev. C* **74**, 045801 (2006)
- [17] A.M. Santos, L. Brito, and C. Providência, *Phys. Rev. C* **77**, 045805 (2008)
- [18] C. Ducoin, C. Providência, A. M. Santos, L. Brito, and P. Chomaz, *Phys. Rev. C* **78**, 055801 (2008)
- [19] H. Pais, A. Santos and C. Providência, *Phys. Rev. C* **80**, 045808 (2009)
- [20] H. Pais, A. Santos, L. Brito, and C. Providência, *Phys. Rev. C* **82**, 025801 (2010)
- [21] H. Pais, A. Sulaksono, B.K. Agrawal, and C. Providência, *Phys. Rev. C* **93**, 045802 (2016)
- [22] H. Pais, and C. Providência, *Phys. Rev. C* **94**, 015808 (2016)

- [23] K. Oyamatsu and K. Iida, *Phys. Rev. C* **75**, 015801 (2007)
- [24] J. Xu, L.W. Chen, B.A. Li, and H.R. Ma, *Astrophys. J.* **697**, 1549 (2009)
- [25] C. Ducoin, J. Margueron, C. Providência, and I. Vidaña, *Phys. Rev. C* **83**, 045810 (2011)
- [26] F. Grill, C. Providência, and S.S. Avancini, *Phys. Rev. C* **85**, 055808 (2012)
- [27] A. Sulaksono, N. Alam, and B.K. Agrawal, *Int. J. Mod. Phys. E* **23**, 1450072 (2014)
- [28] S.S. Bao and H. Shen, *Phys. Rev. C* **89**, 045807 (2014)
- [29] S.S. Bao and H. Shen, *Phys. Rev. C* **91**, 015807 (2015)
- [30] S.N. Wei, R.Y. Yang and W.Z. Jiang, *Chin. Phys. C* **42**, 054103 (2018)
- [31] C. Gonzalez-Boquera, M. Centelles, X. Viñas, and T.R. Routray, *Phys. Rev. C* **100**, 015806 (2019)

TABLE I: The parameters of the Lagrangian for the original DD-PC1 parametrization with parameter $\delta_S = -0.8149$ [fm⁻⁴].

	a_i [fm ⁻²]	b_i [fm ⁻²]	c_i [fm ⁻²]	d_i
$i = S$	-10.0462	-9.1504	-6.4273	1.3724
$i = V$	5.9195	8.8637		0.6584
$i = tV$		1.8360		0.6403

TABLE II: The crust-core transition densities [fm⁻³] for β -equilibrium neutrino-free matter ($Y_\nu = 0$) and neutrino-trapped matter ($Y_l = 0.4$) for several slopes L and temperatures T including $T = 0$ MeV. The results in italic type are for thermodynamical method and the other results are for Vlasov one. Those calculated with the original DD-PC1 parametrization are in bold type.

	L (MeV)	$T=0$ MeV	T=0 MeV	4 MeV	8 MeV	12 MeV
$Y_\nu = 0$	29	<i>0.096</i>	0.091	0.087	0.079	
	42	<i>0.091</i>	0.085	0.077	0.058	
	55	<i>0.086</i>	0.079	0.063		
	70	0.079	0.072			
	86	<i>0.073</i>	0.065			
	103	<i>0.066</i>	0.059			
$Y_l = 0.4$	29	<i>0.095</i>	0.087	0.086	0.081	0.07
	42	<i>0.094</i>	0.086	0.085	0.08	0.068
	55	<i>0.094</i>	0.085	0.084	0.079	0.066
	70	0.093	0.084	0.083	0.078	0.065
	86	<i>0.093</i>	0.084	0.083	0.077	0.063
	103	<i>0.093</i>	0.083	0.082	0.076	0.062

TABLE III: The crust-core transition pressures [MeV fm⁻³] for several slopes L and temperatures T including $T = 0$ MeV. The results in italic type are for thermodynamical method and the other results are for Vlasov one. Those calculated with the original DD-PC1 parametrization are in bold type.

	L (MeV)	$T=0$ MeV	T=0 MeV	4 MeV	8 MeV	12 MeV
$Y_\nu = 0$	29	<i>0.265</i>	0.225	0.275	0.42	
	42	<i>0.417</i>	0.349	0.346	0.378	
	55	<i>0.489</i>	0.393	0.284		
	70	0.485	0.365			
	86	<i>0.404</i>	0.282			
	103	<i>0.283</i>	0.182			
$Y_l = 0.4$	29	<i>1.113</i>	0.93	1.004	1.161	1.242
	42	<i>1.131</i>	0.93	1.006	1.152	1.211
	55	<i>1.148</i>	0.934	1.007	1.144	1.182
	70	1.167	0.936	1.007	1.134	1.151
	86	<i>1.182</i>	0.936	1.004	1.122	1.123
	103	<i>1.192</i>	0.932	0.998	1.108	1.096

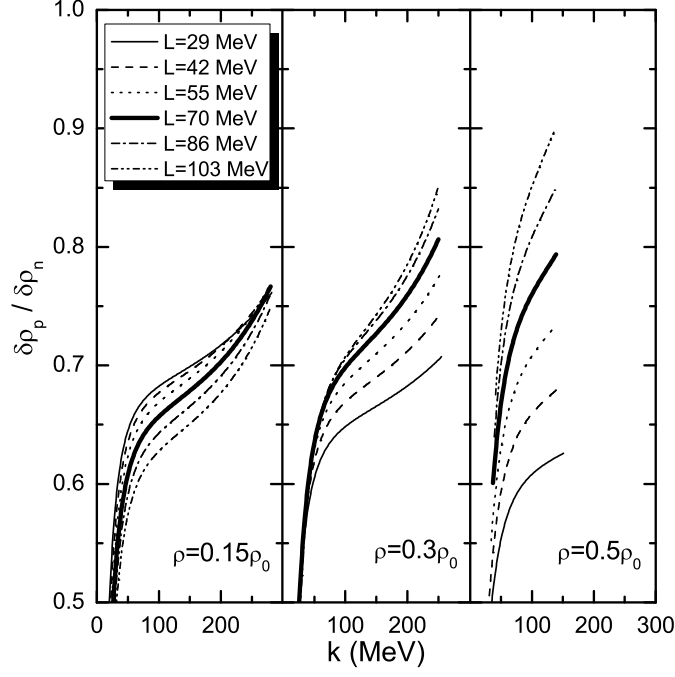


FIG. 1: The ratio of the proton over neutron density fluctuation $\delta\rho_p/\delta\rho_n$ at $T = 4$ MeV plotted for the proton fraction $y_p = 0.3$, for $\rho = 0.15\rho_0, 0.3\rho_0, 0.5\rho_0$, as a function of the wave vector \mathbf{k} . *Thick curves* are for original DD-PC1 parametrization.

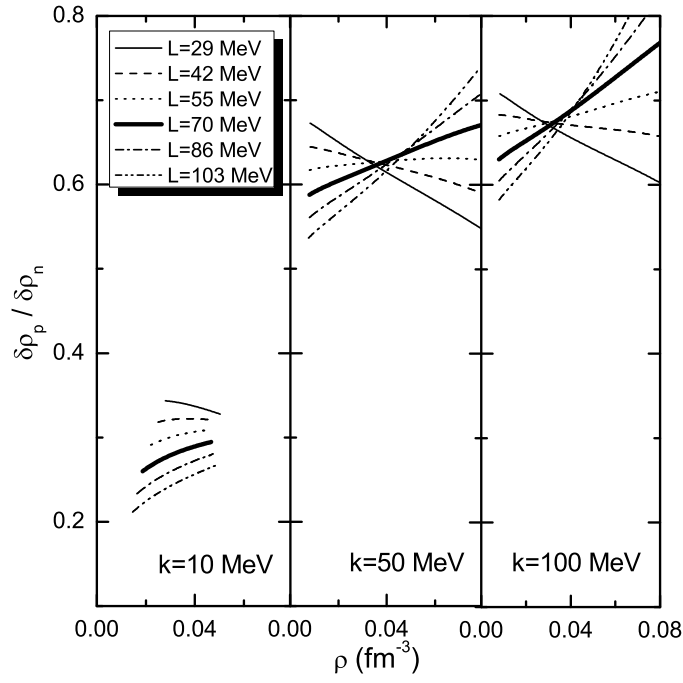


FIG. 2: Same as Fig. 1, but for wave vector $k=10, 50, 100$ MeV as a function of the density ρ . *Thick curves* are for original DD-PC1 parametrization.

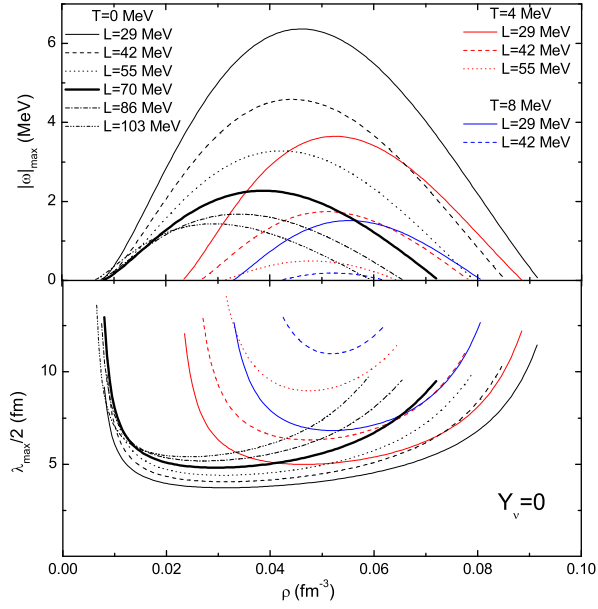


FIG. 3: The growth rate of the most unstable modes (*upper panel*) and corresponding size of clusters (*lower panel*) as a function of density for β -equilibrium neutrino-free matter $Y_\nu = 0$. *Thick curves* are for original DD-PC1 parametrization.

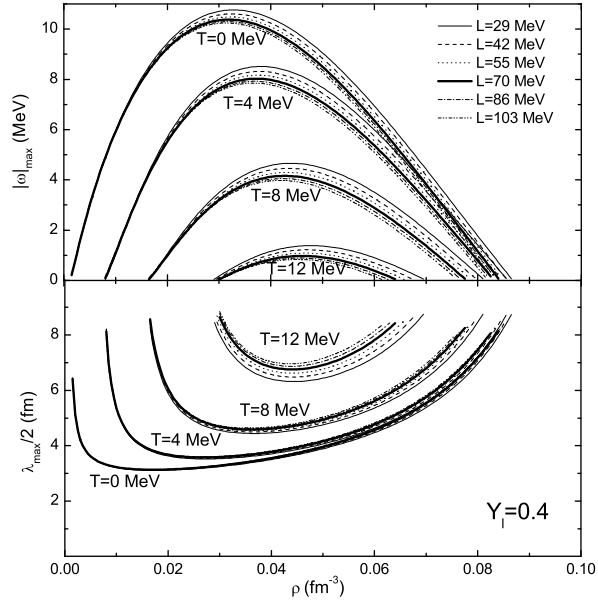


FIG. 4: Same as Fig. 3, but for β -equilibrium neutrino-trapped matter $Y_l = 0.4$. *Thick curves* are for original DD-PC1 parametrization.